

Combining Ultrafast Laser Texturing and Laser Hardening to Enhance Surface Durability by Improving Hardness and Wear Performance

Abhijit Cholkar,* Suman Chatterjee, Sujith Kumar, Marko Sedaček, Bojan Podgornik, David Kinahan, and Dermot Brabazon

Aluminum alloy 7075 is utilized widely across marine, aerospace, and automotive sectors. However, its surface wear resistance has hindered its application in certain tribological environments. Addressing this challenge, the current study examines a hybrid laser method to increase surface wear resistance by combining two techniques: ultrafast laser texturing and laser-based surface hardening. Ultrafast laser processing is conducted using 3 W laser power, 100 kHz pulse repetition rate, 4 mm s⁻¹ scanning speed, and three different scan patterns. After the texturing operation, laser-based surface hardening is then performed on these textures using a continuous wave laser. The laser heat treatment is conducted using laser powers of 400 and 500 W with three different scan speeds of 1, 2, and 3 mm s⁻¹. Microhardness evaluations show a notable increase in hardness, with the hardest sample exhibiting a 17.8% increase compared to the pristine sample. The laser-textured and laser heat-treated samples exhibit a significant reduction in the average coefficient of friction and wear volumes compared to samples that were laser-textured but not laser heat-treated. The investigated laser processing strategy offers a promising approach for surface modification, enhancing both mechanical properties and wear resistance of aluminum alloy 7075 surfaces.

biofouling while enhancing corrosion resistance—a vital necessity in marine settings.^[3,4] Laser texturing has been explored as a technique to enhance the tribological performance of aluminum alloy surfaces.^[5] Studies have shown that laser surface texturing can improve oil retention and reduce the chances of scuffing on sliding surfaces, leading to enhanced operational performance and efficiency.^[6] Laser parameters have been found to significantly affect the size and depth of texture on aluminum alloy surfaces, with dimples acting as solid lubricant reservoirs under solid lubrication.^[7] Laser-induced self-organizing periodic surface structures and deterministic surface textures have been tested for their tribological behavior, with the highest static coefficient of friction (COF) observed for a laser-textured cross pattern, indicating the potential of laser texturing for real-world applications.^[8] Laser-assisted micromachining technologies have also been used to create micro-textures on titanium alloy surfaces, with wavy laser surface texturing showing greater impact on wear resistance capabilities.^[9]

Nevertheless, the rigorous conditions prevalent in extreme marine environments give rise to heightened mechanical wear and tear at multiple locations. Consequently, these surface textures may experience accelerated degradation due to

1. Introduction

Laser texturing has been explored for antifouling applications on aluminum surfaces in the marine industry.^[1,2] This technique demonstrates substantial promise in the development of antifouling surface textures with the capacity to mitigate or preclude


A. Cholkar, S. Chatterjee, S. Kumar, D. Kinahan, D. Brabazon
I-Form, Advanced Manufacturing Research Centre
Dublin City University
Glasnevin, Dublin 9, Ireland
E-mail: abhijit.cholkar2@mail.dcu.ie

A. Cholkar, S. Chatterjee, D. Kinahan, D. Brabazon
Advanced Processing Technology Research Centre, School of Mechanical and Manufacturing Engineering
Dublin City University
Glasnevin, Dublin 9, Ireland

A. Cholkar, D. Kinahan, D. Brabazon
DCU Water Institute, School of Chemical Sciences
Dublin City University
Glasnevin, Dublin 9, Ireland

S. Kumar
Global Innovation and Technology Centre
Transition Optical part of Essilor Luxottica
Tuam, Co. Galway H54 RD25, Ireland

M. Sedaček, B. Podgornik
Metallic Materials and Technology
Institute of Metals and Technology (IMT)
Lepi pot 11, Ljubljana 1000, Slovenia

 The ORCID identification number(s) for the author(s) of this article can be found under <https://doi.org/10.1002/adem.202401183>.

© 2024 The Author(s). Advanced Engineering Materials published by Wiley-VCH GmbH. This is an open access article under the terms of the Creative Commons Attribution License, which permits use, distribution and reproduction in any medium, provided the original work is properly cited.

DOI: 10.1002/adem.202401183

unavoidable environmental stresses. Therefore, it is a necessity to create robust textures that are highly durable. The durability of surface patterns at the contact interface plays a significant role in determining the lifespan of functional properties.^[10,11]

Increasing the life of aluminum surfaces can be achieved through various methods. One study found that the fatigue life of an Al–Mg–Si alloy was improved by polishing the surface, which reduced the size of microporosity and resulted in smaller cracks initiating.^[12] Deep surface rolling (DSR) technology can also increase the fatigue life of metallic materials, including high-strength aluminum alloy, by introducing deep compressive residual stresses in the material surface. In another study, the approach is to use additional heat treatment and deformation, as well as two-stage final annealing, in high-purity aluminum.^[13] In another study, MXene nanosheets are used in combination with laser textures which improve the wear resistance and durability of the components.^[14,15] However, the stability of MXene coatings is not as good as other physical methods.^[16]

Laser beam hardening has been recognized in prior research as a promising technique for enhancing hardness and prolonging wear resistance.^[17–19] Yang et al. discussed the effects of laser heat treatment on the surface of aluminum alloy, which resulted in improved local hardness and optimized corrosion resistance. Laser treatment reduced the number and continuity of pitting pits on the surface of the alloy and decreased intergranular corrosion and maximum corrosion depth.^[20] Tolcha et al. investigated laser surface alloying of pure aluminum, which resulted in increased hardness and improved wear resistance of the alloyed zones.^[21] By combining laser texturing and laser hardening, it is possible to achieve both improved surface hardness and modified surface topography and chemistry.^[22] This combination can be used to create surfaces with increased roughness and enhanced adhesion, as well as to improve lubrication and wear behavior.^[23] Combining the process of laser hardening and laser texturing involves using laser texturing to modify the surface topography and then applying laser hardening to produce hardened surfaces with the desired properties.^[24] Surface roughness attributes influence the tribological properties such as wear. In practice, the most used parameters for surface roughness description are S_a , S_q , S_{sk} , and S_{ku} . Average surface roughness (S_a) offers a comprehensive characterization of height deviations but lacks sensitivity to subtle profile changes and waviness. Root mean square deviation (S_q) is more responsive to deviations from the baseline than S_a . Skewness (S_{sk}) quantifies asymmetry, with zero indicating symmetrical height distribution, positive values indicating high peaks or filled valleys, and negative values indicating deep scratches or loss of peaks. Conversely, kurtosis (S_{ku}) reflects the sharpness of the profile's probability density.^[25,26]

Ultrafast laser texturing has been proven effective in enhancing the wear resistance of aluminum alloys. Research has shown that femtosecond laser processing of micro-textures on aluminum alloy surfaces can significantly improve friction properties, with optimal drag reduction achieved at an area ratio of around 8% and a drag reduction of 36.76% compared to non-textured surfaces.^[27] Combining ultrafast laser texturing with laser hardening presents substantial advantages for surface functionalization and durability enhancement.^[28,29] Ultrafast laser texturing enables the precise formation of micro- and nanostructures on various substrates, thereby influencing key properties such

as hydrophobicity, wear resistance, and tribological behavior. Concurrently, laser hardening enhances the mechanical properties of surfaces, significantly improving their resistance to wear and deformation. The integration of these two techniques facilitates the creation of textured surfaces with superior mechanical strength and wear resistance, making them suitable for applications demanding both functional surface properties and durability.^[30]

From the literature mentioned earlier, it was found that the investigations of these two techniques, femtosecond laser texturing and laser hardening, are reported independent of each other. The majority of researchers have concentrated on either one aspect or the other in order to enhance performance. The synergistic effect of both techniques has not previously been explored or reported in detail. In our previous research,^[4] we investigated a variety of surface textures to evaluate their antifouling and corrosion-resistant properties. From this previous study, we identified specific textures that demonstrated significant biofilm inhibition. These textures exhibited promising potential in mitigating biofouling and enhancing corrosion resistance. Consequently, these identified textures with superior biofilm inhibition properties were selected for further examination in the present study. We hypothesize that the continuous wave laser hardening process can be used to enhance the mechanical surface properties for ultrafast laser-textured samples and specifically that samples processed via this multimodal approach would exhibit a better wear resistance. Therefore, we explore the effect of multimodal laser texturing in this study. Three laser textures were fabricated using femtosecond laser processing. Laser hardening was conducted on these samples with varying laser process parameters. The hardness and wear resistance were explored on each sample produced with the different parametric settings.

2. Experimental Section

2.1. Material

The material used in this project was commercially available aluminum alloy 7075 T6 (thermally treated, stress-relieved by stretching, and artificially aged), in the form of flat plates with 100 × 30 mm and 2 mm thick which are supplied by Impact Ireland Metals Ltd. The average roughness (S_a) of the bare plate was 400–500 nm before processing as measured by 3D optical profilometer. The surface of the samples was cleaned using isopropyl alcohol before laser processing. The chemical composition of the aluminum alloy 7075 is shown in **Table 1**.

2.2. Laser Surface Texturing

The ultrafast laser surface texturing was conducted on the aluminum alloy 7075 substrates using a laser system which was equipped with a high-energy industrial ultrafast laser source (NKT Photonics Origami XP). This laser provides a stable

Table 1. Chemical composition of aluminum alloy substrates 7075.

Material	Zn	Mg	Cu	Si	Mn	Fe	Ti	Al
Aluminum alloy 7075	5.8	2.8	1.5	0.1	0.17	0.22	0.03	Balance

low-noise pulsed beam with an average wavelength of 1030 nm and a pulse duration <math><370\text{ fs}</math>. The laser beam surface scanning with different pattern designs was conducted with a galvo scanner (Focusshifter-15, Raylase GmbH), and the beam was focused on the sample using an f-theta lens. Gaussian type of beam was present at the focal position which had a full width of the beam at $1/e^2</math> measured to be $46.4\text{ }\mu\text{m}</math> at a working distance of 220 mm from the lens of the galvo scanner. The laser texture scanning pattern was applied across an irradiated area of $8 \times 8\text{ mm}</math> (Figure 1).$$$

The laser processing was conducted in the atmospheric environment at $20\text{ }^\circ\text{C}</math> and 60 relative humidity. In this experiment, the laser texturing process parameters were set as 3 W laser power, 100 kHz pulse repetition rate, and $4\text{ mm s}^{-1}</math> scanning speed. The fluence of $1.77\text{ J cm}^{-2}</math> was kept constant in the experiments. These parameters were selected based on our previous study to optimize parameters to improve surface properties.^[31]$$$

The surface heat treatment of the laser-textured samples was conducted, after laser texturing was performed, using a water-cooled continuous wave fiber laser source (IPG YLR 1000 WC). This laser provides a stable low-noise beam with an average wavelength of 1070 nm. The rectangular beam of $6 \times 6\text{ mm}</math> was used with beam mode quality ($M2 < 1.1</math>). The sample was mounted on the 4-axis translation stage (PRO 225 Aerotech Inc). The laser was focused on the top surface of the sample on which the laser-textured samples were present. The stage was calibrated and was translated in the different set speeds as represented in Figure 2. due to which the laser beam was scanned over the sample. The experimental setup involved varying the laser power and scanning speed to fabricate-textured surfaces on aluminum substrates. Two laser powers, 400 and 500 W, were utilized in conjunction with three scanning speeds of 1, 2, and $3\text{ mm s}^{-1}</math>. These parameters were selected based on preliminary pilot tests$$$

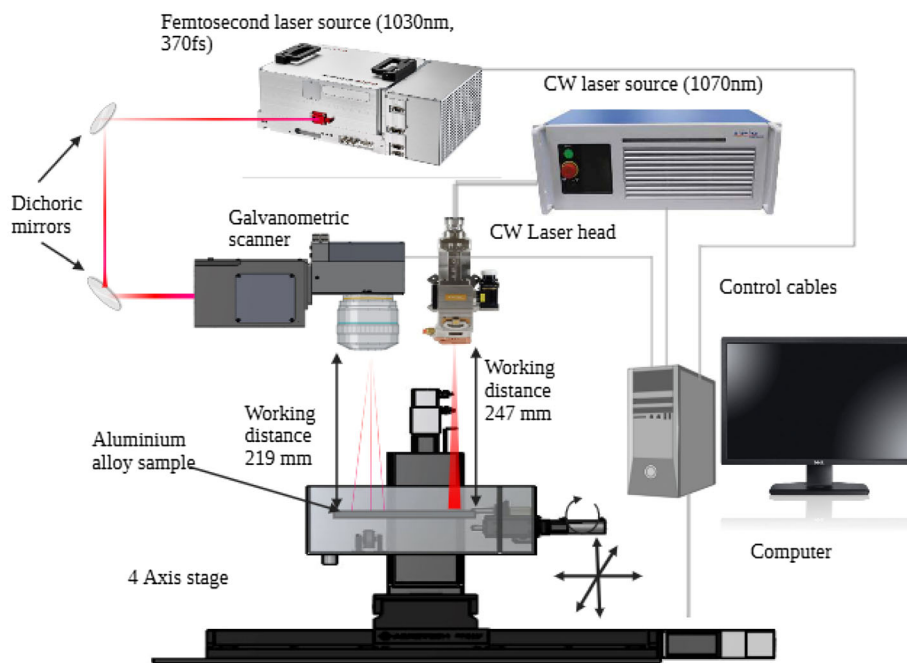


Figure 1. Multimodal laser surface texturing and hardening setup.

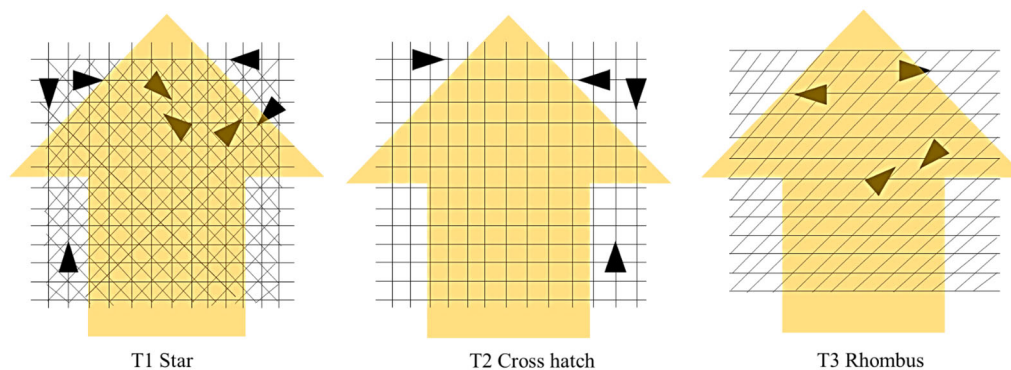


Figure 2. Schematic of the different scan patterns implemented for femtosecond laser texturing in black (laser spot size of $46.4\text{ }\mu\text{m}</math>) and the CW laser for hardening (laser spot size $6\text{ mm} \times 6\text{ mm}</math>) in yellow.$$

Table 2. The design of experiments laser process parameters and levels examined.

Parameter	Unit	Level 1	Level 2	Level 3
A Laser power (P)	W	400	500	–
B Scan speed (h)	mm s ⁻¹	1	2	3
C Texture	–	T1 (Star)	T2 (Square)	T3 (Rhombus)

Table 3. Full listing of the process parameters and associated levels investigated for each sample.

Sample no	Laser process parameter setting		
	Power [W]	Scan speed [mm s ⁻¹]	Texture
1	400	1	T1
2	400	1	T2
3	400	1	T3
4	400	2	T1
5	400	2	T2
6	400	2	T3
7	400	3	T1
8	400	3	T2
9	400	3	T3
10	500	1	T1
11	500	1	T2
12	500	1	T3
13	500	2	T1
14	500	2	T2
15	500	2	T3
16	500	3	T1
17	500	3	T2
18	500	3	T3

conducted on both plain and textured surfaces to ensure optimal process conditions. Initial pilot experiments revealed that below 400 W of power, there was minimal lasting effect due to significant reflection of the incident laser beam by the aluminum surface. Consequently, the energy deposition was insufficient to induce noticeable surface modifications. Conversely, when the laser power exceeded 500 W, distortion and crack formation were observed on the textured surfaces which compromised the integrity of the surface. Additionally, the range of scanning speeds encompassing 1–mm s⁻¹ was selected to provide flexibility in controlling the traversal rate of the laser beam across the substrate surface (Table 2). Therefore, in total, 18 samples with distinct parameter setting were fabricated in this experiment. Table 3 shows full listing of the process parameters and associated levels investigated for each sample.

2.3. Surface Characterization and Wear Experiments

2.3.1. Morphology and Surface Chemistry

The laser-treated surfaces were evaluated using scanning electron microscopy using an EVO LS15 instrument (Zeiss)

equipped with a LaB6 filament, operating at an accelerating voltage of 10 kV and a beam current intensity of 25 pA. The evaluation was conducted in secondary electron diffraction mode. The images were taken at 100X and 1000X magnification for all the patterns. As the aluminum alloy samples are conductive, no extra sample coating was required. The surface chemistry was analyzed using the Oxford Instruments energy-dispersive spectroscopy (EDS) system (Aztec).

2.3.2. Surface Roughness

The different surface roughness height attributes such as S_a (arithmetical mean height), S_q (root mean square surface roughness), S_{ku} (kurtosis) and S_{sk} (skewness) were characterized using a Bruker Contour GT 3D Optical Profilometer as per ISO standard 25178-2:2021.^[32] The measurements were made using a 10X lens and focusing on the sample using white light interferometry. The analysis of the surface roughness parameters was performed using inbuilt software Bruker's Vision 64 image analysis on the raw data.

2.3.3. Microhardness

The micro-indentation tests were conducted using the NHT3 (Anton Paar). In order to pursue a mechanical property evaluation at micrometer scale, instrumented micro-indentation was performed on all the laser-processed samples. The load control mode was used to perform the micro-indentation-based analysis. Indentation was performed at maximum indentation load (P_{max}) of 1500 mN with loading–unloading time of 30 s each. Hold time of 10 s is used at P_{max} to avoid the influence of creep on the hardness measurement. Standard geometrically similar four-sided Vickers indenter with tip radius of ≈ 200 nm was used for the experimentation. Prior to indentation, area function of the indenter was calibrated using standard fused silica sample. Five indentations were performed on each sample to obtain a statically significant data.

2.3.4. Wear Resistance

Friction and wear testing were performed under reciprocating sliding contact using ball-on-disk contact configuration and water drop lubrication. Tests were performed at room temperature (22 ± 2 °C) and relative humidity of $50 \pm 5\%$. Before each test, specimens were cleaned in ethanol and dried in air, and a drop of distilled water (≈ 0.02 mL) is applied on the Al disk surface. Standard 100Cr6 bearing steel ball ($\phi 20$ mm, 58 HRC) was used as a stationary counter-body, pressed against an oscillating Al flat sample. Oscillating frequency and amplitude were 15 Hz and 4 mm, respectively, resulting in the average sliding speed of 0.12 m s⁻¹. Normal load applied was 10 N, corresponding to the initial Hertz contact pressure of 400 MPa. Testing was performed for 600 s, which resulted in the total sliding distance of 72 m. During testing, COF was recorded continuously as a function of time. After the test, average steady-state COF was calculated, and wear volume of the Al disks is measured and analyzed using 3D focus variation microscope Alicona InfiniteFocus G4.

3. Results and Discussion

3.1. Surface Micrograph and Surface Chemistry

Three different textures were created on aluminum samples using femtosecond laser system using 3 W laser power, 100 kHz pulse repetition rate, and 4 mm s⁻¹ scanning speed with constant fluence of 1.77 J cm⁻². The above textures were applied as these already have antifouling ability as per our previous study.^[33] The above pictures show the microtextured surfaces before laser hardening and after laser hardening process. In **Figure 3a,b**, the observed morphologies displayed a star-shaped pattern (T1) characterized by numerous radial projections emanating from a central locus, exhibiting notable regularity in spacing. Microscopic examination at high magnification revealed intricate surface features along the projections, alongside a comparatively diminutive region lacking such textural complexity. Coarse textures with nanoscale features were observed on the micrometer scale surface textures due to the evaporation and recrystallization on the top of the surface. Subsequent to the laser surface hardening, the laser tracks resulting from the femtosecond laser processing have almost disappeared; however, the periodicity and geometric features have not changed. In **Figure 3c**, the cross-hatched pattern (T2), the generation of straight parallel and perpendicular incisions was observed. This scanning methodology led to a notable augmentation in surface area. Predominantly, nano- and microscale structures were generated along the crown region of the surface, resulting in a heightened surface area. **Figure 3d** shows the laser hardened cross-hatched texture. The protrusion on the texture has reduced after the laser scan without

disturbing the periodicity and geometric attributes. A boundary-type feature was generated on the star and square textures after laser surface hardening of the femtosecond laser texturing, as shown in **Figure 3b,d**. An oxide layer can be seen to have been produced on this coarse boundary of the texture. The presence of an oxide layer on the boundary of the texture is attributed to the recrystallization involved during the laser heat treatment process. As the laser interacts with the material surface, it generates localized heating, causing oxidation of the material at the textured boundaries.^[34] This thermal effect induces the formation of oxide layers, altering the surface characteristics. **Figure 3e** exhibits a discernible rhombus-shaped pattern, characterized by the presence of interconnected geometric units forming a series of rhombus across the observed surface. These rhombuses had an angle of 45°. **Figure 3f** shows the texture after the laser hardening. A coarse cauliflower-like surface texture boundary was formed adjacent to the texture which is similar to that reported previously in the literature after hardening is formed.^[35] The surface chemistry characterization was conducted using EDS. The surface compositions of the laser-textured and hardened samples, measured using the EDS, are presented in **Table 4**.

3.2. Effect of Multimodal Laser Texturing on Surface Roughness

Laser texturing and hardening produce textures which have different surface roughness values. The roughness depends on the scanning strategy and the laser parameters of both texturing operation and laser parameters of laser hardening operation.

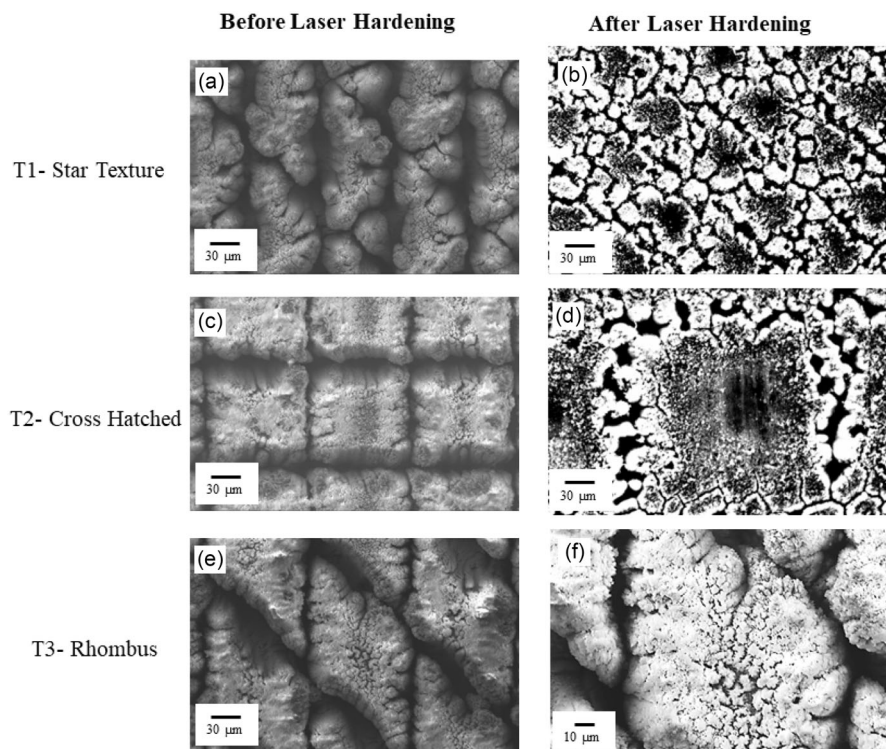


Figure 3. SEM of different laser textures on the aluminum alloys before and after the laser hardening treatment: a,b) Star texture; c,d) Cross hatched texture; and e,f) Rhombus texture.

Table 4. EDS results measured from the ultrafast laser-textured and hardened aluminum surface.

Sample	C [%]	O [%]	Al [%]	Fe [%]	Cu [%]	Mg [%]	Zn [%]
Prestine	4.34	6.28	79.04	0.22	1.5	2.8	4.92
Sample 1 (T1)	4.48	42.93	52.2	0.39	0	0	0
Sample 2 (T2)	4.79	33.05	52.85	0.50	1.16	2.8	4.86
Sample 3 (T3)	4.25	35.49	50.94	0	0.95	2.82	0.24

Various roughness attributes stated in the previous research^[25] such as S_a (arithmetical mean height), S_q (root mean square surface roughness), S_{ku} (kurtosis), and S_{sk} (skewness) are characterized. **Figure 4** shows the surface roughness attributes for each laser-textured and heat-treated sample.

The pristine (non-textured) sample of Al 7075 had surface roughness values S_a $0.43 \pm 0.0006 \mu\text{m}$, S_q $0.52 \pm 0.001 \mu\text{m}$,

S_{ku} 2.59 ± 0.03 , and S_{sk} 0.24 ± 0.008 . Non-heat-treated femtosecond laser-textured sample of Al 7075 with star texture (T1) had surface roughness values S_a $7.99 \pm 0.0006 \mu\text{m}$, S_q 14.76 ± 0.02 , S_{ku} $14.22 \pm 0.04 \mu\text{m}$, and S_{sk} 3.12 ± 0.014 . Sample with cross-hatched texture (T2) had surface roughness values S_a $4.16 \pm 0.02 \mu\text{m}$, S_q $5.91 \pm 0.03 \mu\text{m}$, S_{ku} 29.16 ± 0.03 , and S_{sk} 2.93 ± 0.018 . Sample with rhombus texture (T3) had surface roughness values S_a $6.39 \pm 0.09 \mu\text{m}$, S_q $11.52 \pm 0.015 \mu\text{m}$, S_{ku} 18.68 ± 0.015 , and S_{sk} 3.72 ± 0.014 . **Figure 4** displays the comprehensive results pertaining to the surface roughness attributes. Notably, sample 9 exhibits the highest values of S_a and S_q , while samples 7 and 16 demonstrate the lowest and highest values, respectively, within this context. Regarding skewness and kurtosis of surface roughness, sample 17 attains the lowest values, whereas sample 13 exhibits the highest values in this regard. Also, it can be observed that for most of the samples, the surface roughness reduces after the heat treatment which affects the wear performance.^[34]

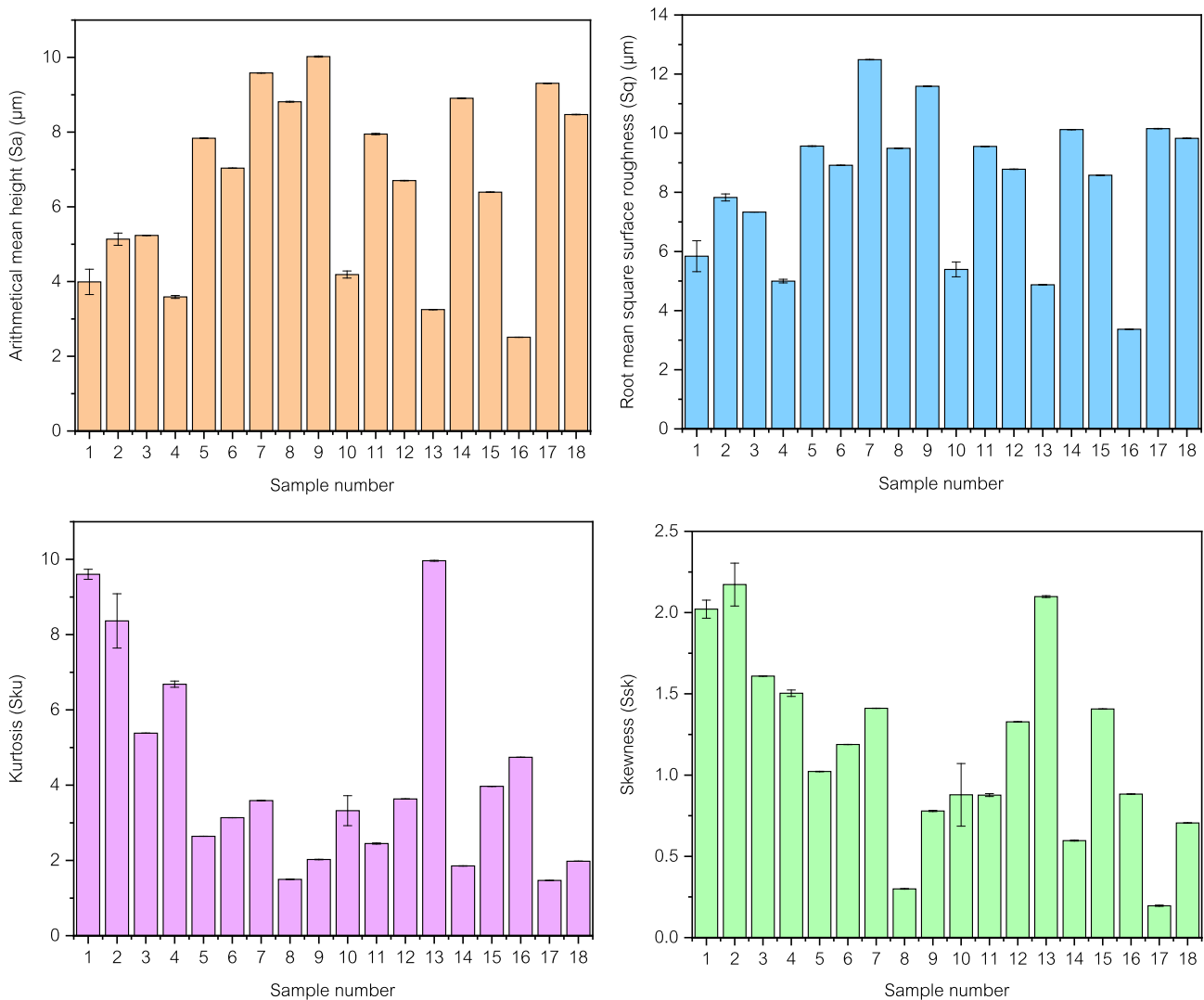


Figure 4. Distribution of surface roughness attributes S_a (arithmetical mean height), S_q (root mean square surface roughness), S_{ku} (kurtosis), and S_{sk} (skewness) of laser-textured and heat-treated samples.

Three different laser scanning strategies namely star hatch pattern, cross-hatched pattern, and rhombus pattern have been studied to understand their effects on surface morphology in laser surface texturing and hardening using an ultrafast laser system and heat treatment laser system. As the samples had constant parameters for texturing, only the influence of the laser heat treatment was observed in this study. Clearly, it can be seen that the surface finish analysis of the textured and heat-treated reveals that alterations in laser parameters exert a substantial influence on the absorption of laser radiation, resulting in considerable variability in roughness values. Additionally, the phenomena of laser heat treatment and recrystallization of the textures are observed to occur. In some samples, surface distortion at higher power and lower speeds was also observed which resulted in high skewness and highly sharp textures with peaks and valleys. The influence of laser parameters such as laser power and scan speed and the influence of different textures (created by femtosecond laser texturing with constant parameters) are conducted using 3-level full factorial experimental design technique. Four mathematical models were developed for roughness attributes using response surface methods. The details of the ANOVA are provided in the Supporting Information. Two numerical factors and one categorical factor were used in this study.

The regression equation derived for S_a , S_q , S_{ku} , and S_{sk} is as follows:

$$S_a = 6.6070 + 1.292055B - 2.08809C[1] + 1.3842C[2] - 1.05094AB - 1.0044AC[1] + 0.9275AC[2] \quad (1)$$

$$S_q = 8.2613 + 1.0155B - 2.1009C[1] + 1.190955C[2] - 1.0790875AB - 1.2041AC[1] + 0.9019AC[2] \quad (2)$$

$$S_{ku} = 4.2388 - 1.4545B + 2.0779C[1] - 1.1930C[2] + 1.2518AB \quad (3)$$

$$S_{sk} = 1.1654 - 0.3842B + 0.3005C[1] - 0.3047C[2] - 0.2853AB^2 \quad (4)$$

where A is the laser power in (W), B is the scan speed in (mm s^{-1}), $C[1]$ is the star texture (T1), $C[2]$ is the cross-hatched texture (T2), and $C[3]$ is the rhombus texture (T3). The concordance between this model and the empirical data was assessed using both a normal plot of the residuals and a plot comparing predicted values to actual values (refer to Supporting Information). The response surface 3D plots are plotted using the derived regression equations showing the effect of laser hardening parameters in **Figure 5**.

The surface roughness attributes such as S_a (arithmetical mean height), S_q (root mean square surface roughness), S_{ku} (kurtosis), and S_{sk} (skewness) are significantly affected by the laser hardening process parameters. Laser scanning was identified as the most influential parameter on the average height roughness (S_a) parameters, with a direct relationship. It can be seen that the increase in scan speed leads to an increase in average height roughness. The time of interaction of the laser beam and cooling rate during the hardening process influence the irregularities in the peak and valley of the surface texture.

These findings align with previously documented results as reported in prior studies by Erinoshio et al. on copper surface.^[36] Evidently, a similar trend is seen in terms of root mean square surface roughness (S_q). However, the lower scan speed produces higher kurtosis surface roughness which shows the effect of degradation of the surface texture and surface deformation. The increase in laser power also results in deformation of the surface because of melting. The skewness is also higher at lower speed and lower power. However, the higher scan speed and laser power produces lower skewness. These findings are similar to study by Ürgün et al.^[37] The agreement of this model with the experimental results was evaluated with normal plot of the residuals and a plot of the predicted versus actual values (see Supporting Information). It can be seen from these graphs that deviations from the model are approximately normal, and there are no significant outliers in either dataset.

3.3. Effect of Multimodal Laser Texturing on Microhardness

To evaluate the mechanical response of laser-processed and heat-treated aluminum 7075 samples, indentation response of the material is evaluated using standard indentation load versus indentation depth ($P-h$) curve. The indentation was done on the arbitrary locations on the sample. The hardness of all the samples is measured as per Oliver and Pharr method (OPM). **Figure 6a,b** shows the characteristics terms associated with hardness measurement using OPM. By following OPM, first, H of both the systems are assessed using the following relation

$$H = \frac{P_{\max}}{A_c} \quad (5)$$

In the above relation, A_c signifies the contact area of indentation. A_c is estimated using the relation $3\sqrt{3} h_c^2 \tan^2 \theta$, where h_c is the contact depth of indentation and θ is the angle of indentation. The hardness value of the pristine sample of Al 7075 without any texture was 1097 MPa.

The results in **Figure 6** indicate that eight samples underwent a process of hardening, whereas the remaining ten samples exhibited softening, which could be attributed to the effect of melting induced by elevated heat input and laser material interaction.^[38] Notably, the sample denoted as sample 10, fabricated utilizing laser power of 500 W with a scan speed of 2 mm s^{-1} and featuring a texture (T1) characterized by a star pattern, exhibited the highest hardness. This sample manifested no distortion and achieved a hardness value of 1291.90 ± 178.19 . The microhardness was increased by 17.8% compared to the pristine specimen. However, the sample identified as sample 16, produced with laser power of 400 W and a scan speed of 1 mm s^{-1} with star pattern texture (T1), showed the lowest hardness due to heightened interaction resulting from the lower speed, consequently leading to softening.

A cubic model was developed to find out the relationship between laser hardening processing parameters and the resulting hardness. The details of the ANOVA are provided in the Supporting Information. The regression equation developed is as follows

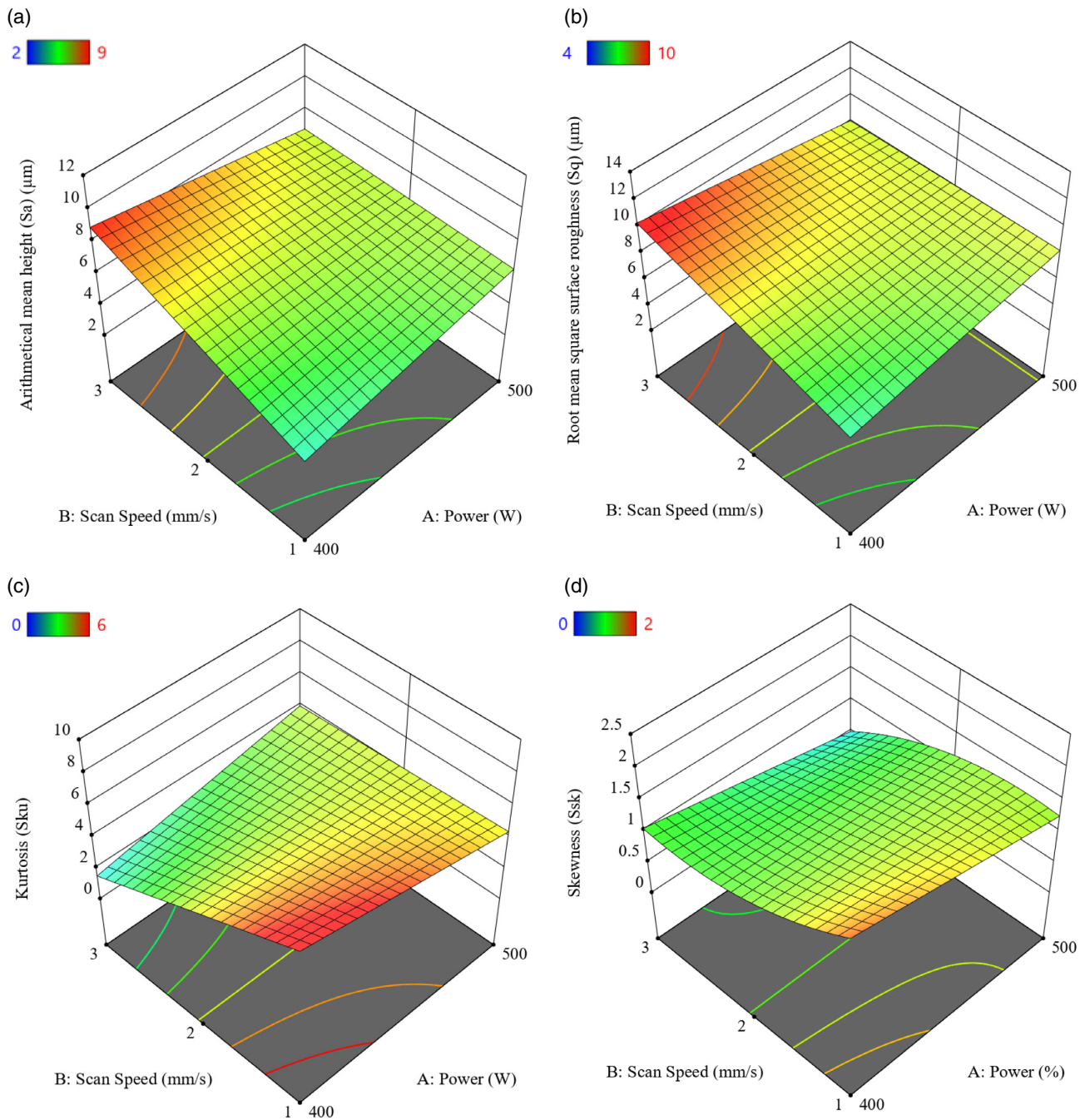


Figure 5. Effect of laser hardening parameters such as laser power (W) and scan speed (mm s^{-1}) on different surface roughness attributes such as a) S_a (arithmetical mean height), b) S_q (root mean square surface roughness), c) S_{ku} (kurtosis), and d) S_{sk} (skewness).

$$\begin{aligned} \text{Microhardness} = & 847.0696 - 122.035A - 73.9885B \\ & + 13.8296C[1] - 9.2975C[2] - 147.6695AB \\ & - 29.9283AC[1] + 77.2385AC[2] \\ & - 83.6814BC[1] + 98.3738BC[2] \\ & + 211.1657B^2 + 70.2447AB^2 \end{aligned}$$

where A is the laser power in (W), B is the scan speed in (mm s^{-1}), $C[1]$ is the star texture (T1), $C[2]$ is the cross-hatched texture (T2), and $C[3]$ is the rhombus texture (T3).

The contour plot in **Figure 7** was plotted using the above regression equation and shows the distribution of microhardness with respect to laser scan speed (mm s^{-1}) and laser power (W) set. It can be seen that higher hardness can be achieved at low speed and high power; however, distortion can occur on

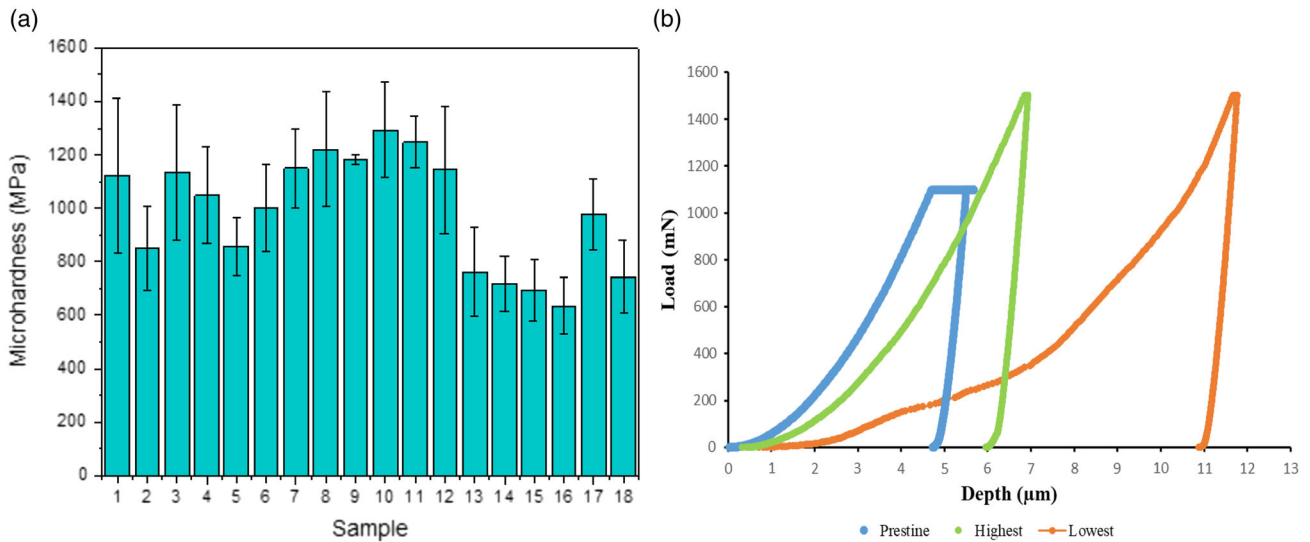


Figure 6. a) Measured microhardness of each laser-textured and hardened sample. Error bars shown are 95% CIs ($n = 5$); and b) load versus indentation depth plotting for the pristine (blue), hardest (green), and least hard (orange) specimens.

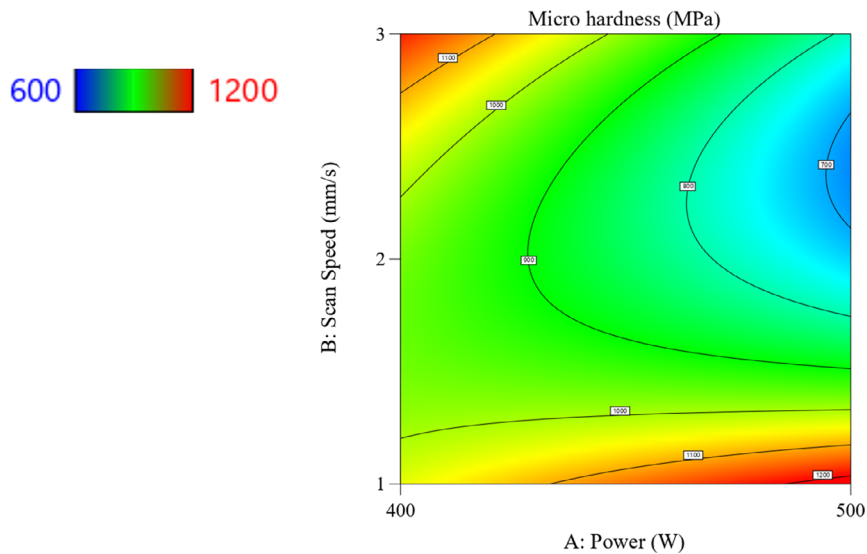


Figure 7. Contour plot showing the distribution of microhardness with respect to laser hardening process parameters power and scan speed.

surface in this condition. On other hand, at lower power and higher speed, the higher hardness can be achieved. This finding is in consistency with previous findings by Barka et al.^[39] The agreement of this model with the experimental results was evaluated with the aid of a normal plot of the residuals and a plot of the predicted versus actual values (see Supporting Information). It can be seen from these predicated versus actual plots in the Supporting Information that the developed model was able to predict the output response effectively and was statistically significant.

3.4. Effect of Multimodal Laser Texturing on Tribological Properties

3.4.1. Analysis of the Coefficient of Friction

The reciprocating sliding wear test was conducted on all the non-heat-treated and heat-treated samples. Non-heat-treated Al 7075 (T1) shows initial friction of about 0.9. After the running-in period of 150–200 s, COF reaches steady-state value of about 1.8, although still showing slight upward trend as shown in

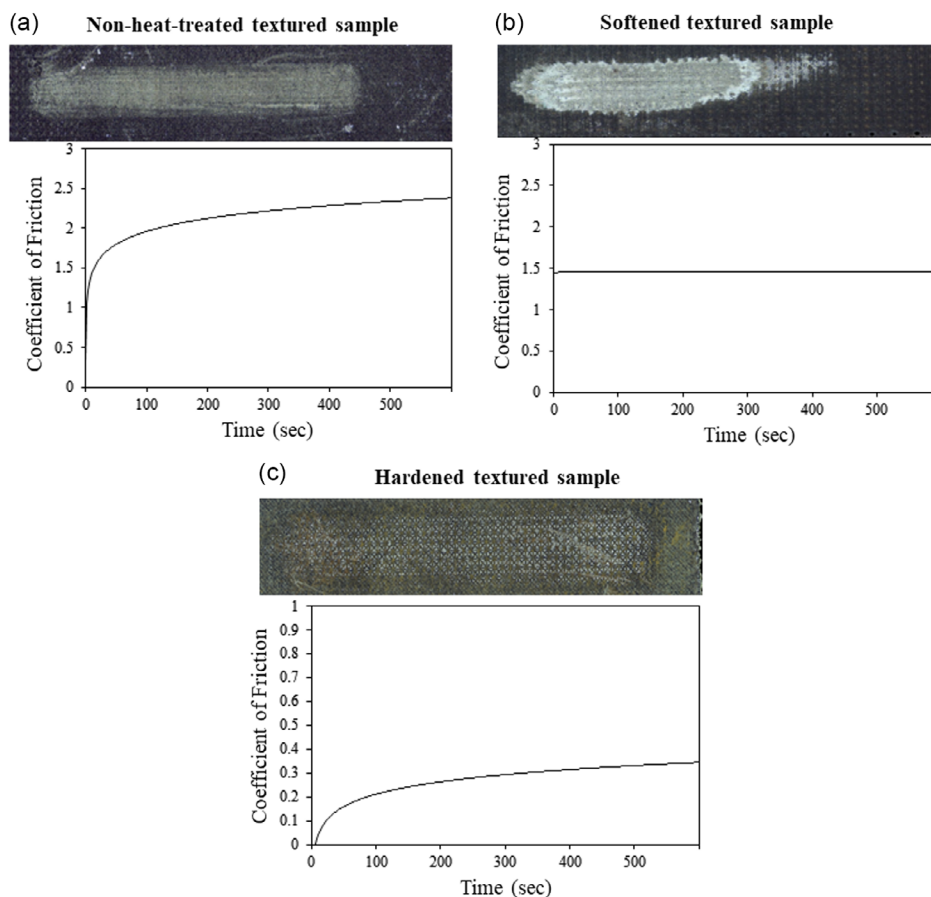


Figure 8. a) Wear scars and corresponding COF trend plotted in log scale versus time curve for non-heat-treated textured surface, b) wear scars and corresponding COF versus time curve for heat-treated textured surface with laser power 400 W, scan speed of 1 mm s⁻¹, and texture T1, and c) wear scars and corresponding COF versus time curve for heat-treated textured surface with laser power 500 W, scan speed of 1 mm s⁻¹, and texture T1.

Figure 8a. The corresponding wear scar is also shown which shows the worn texture having adhesive marks. When the textured surface was treated with laser heat treatment using CW laser, both hardening and softening were achieved. The amount of hardening and softening of surface depends on the laser process parameters. On sample 16 as depicted in Figure 8b with process parameters (laser power 400 W, scan speed of 1 mm s⁻¹, and star texture (T1)), the steady-state friction of about 1.5 was reached at the very beginning of the test without pronounced running-in period. In this case, COF showed a very slight rise during the wear test. The corresponding image shows the wear scar with almost all texture removed along with adhesive and abrasive wear marks. The overall friction coefficient was reduced by 16%; however, the textures on specimen are destroyed at the wear tracks. This could be the effect of wear and surface smoothing. When a laser-textured surface is hardened using the process parameters of laser power 500 W, scan speed of 2 mm s⁻¹, and star texture (T1), this sample is the hardest sample as per the previous section. In this sample, initial friction is 0.09. After running-in period of about 300 s, the steady state was reached with friction of about 0.3. The overall friction coefficient was reduced by 83% compared to the non-heat-treated sample. The results of the friction

coefficient of this specimen are as shown in Figure 8c. Highly effective reduction is obtained in this specimen than all other specimens.

Based on the observed outcomes of friction and wear track analysis across various sliding stages, it is deduced that the reduction in friction behavior of Al 7075 alloys after ultrafast laser treatment can be attributed to the combined impacts of laser texturing and the formation of a laser-induced hardened layer. During the initial sliding stages, the presence of surface textures leads to a reduction in the effective contact area between the matrix and friction couples, thereby mitigating stiction.^[40] The ploughing effects triggered by this debris caused during sliding could lead to more significant damage to the substrate. However, surface textures could mitigate this adverse influence through their ability to trap this debris.^[41] From the results presented in Figure 8, it can also exert a critical effect on the friction performance improvement. To observe the effect of the laser process parameters, all the results of the samples were analyzed, and their average COFs were calculated. These values were put into the experimental design to generate a model to find out the relationship between the average COF with the hardening laser process parameters. The regression equation of the model is as follows

$$\text{Coefficient of friction} = 0.56287 - 0.3647A - 0.36065B + 0.4029AB \quad (7)$$

where A is the laser power in (W) and B is the scan speed in (mm s^{-1}).

From the response 3D surface plot in **Figure 9**, it is clear that COF of 7075 Al alloy is significantly affected by the laser hardening process parameters. As it can be observed, the COF is higher at low power and low scan speed (400 W power, and 1 mm s^{-1} scan speed). Whereas at higher power and higher speed (500 W power, 3 mm s^{-1} scan speed), the COF is reduced. In accordance with the findings delineated in the preceding section, optimal hardness is attained through the employment of specific laser processing parameters, namely 500 W laser power coupled with a scan speed of 2 mm s^{-1} . This configuration corresponds to a notably diminished average COF, quantified at 0.22. Remarkably, this represents a substantial reduction of 76% in the COF compared to the singularly textured sample. The higher the coefficient of friction, the lower is the wear resistance expected.^[42]

3.4.2. Wear Volume

The wear volume of the Al 7075 plates was measured and analyzed using a 3D focus variation microscope. The main wear mechanism for all specimens, untreated and laser-textured and hardened, was sliding wear, combining adhesive and abrasive wear, and surface smoothening. The wear volume for untreated Al7075 alloy was $2.37 \times 10^6 \text{ mm}^3$. The volume measured on each sample is illustrated in **Figure 10**.

Figure 10 shows the wear volumes. The non-heat-treated laser textured samples with textures T1, T2, and T3 had wear volumes of 0.0023, 0.0026 and 0.0027 mm^3 , respectively. In some cases, it was impossible to get representative wear volumes, but this was mainly due to specimen deformation. The abrasive nature of the

wear process altered the shape or structure of the specimens, making it harder to measure wear volumes accurately and reliably. Laser heat treated samples 1, 2, and 3 were manufactured with laser power 400 W and scan speeds of 1, 2, and 3 mm s^{-1} . On samples 10 and 11, on the other hand, there was negligible wear; therefore, the laser textures were unaffected by sliding wear. There was no wear removal in 600 cycles, assuming the wear volume as a maximum of 0.007 mm^3 for deformed conditions and negligible wear condition as 0. These values were put into the experimental design to generate a model to find out the relationship between the wear volumes with the hardening laser process parameters. The regression equation of the model is as follows:

$$\text{Wear Volume} = 0.00167 - 0.0009A + 0.00066AB + 0.00187B^2 - 0.0014AB^2 \quad (8)$$

From the response plot in **Figure 11**, it can be seen that the lowest wear volume is present in the blue region which is 500 W and lies between 1 and 2 mm s^{-1} scan speed. This blue region indicates the laser process parameters with the most wear-resistant characteristics. The specific laser processing parameters used for surface texturing and hardening, such as laser power and scan speed, are optimized to achieve the desired surface characteristics that minimize wear. In this case, the parameters used for sample 10 are ideal leading to a notable reduction in wear volume compared to the untreated specimens. Hence, the anticipated enhancement in mechanical performance can be attained through a judicious selection of processing parameters.

3.5. Correlation between roughness, hardness, coefficient of friction, and wear volume

To explore potential relationships between input process parameters and their corresponding responses, we employed Pearson's

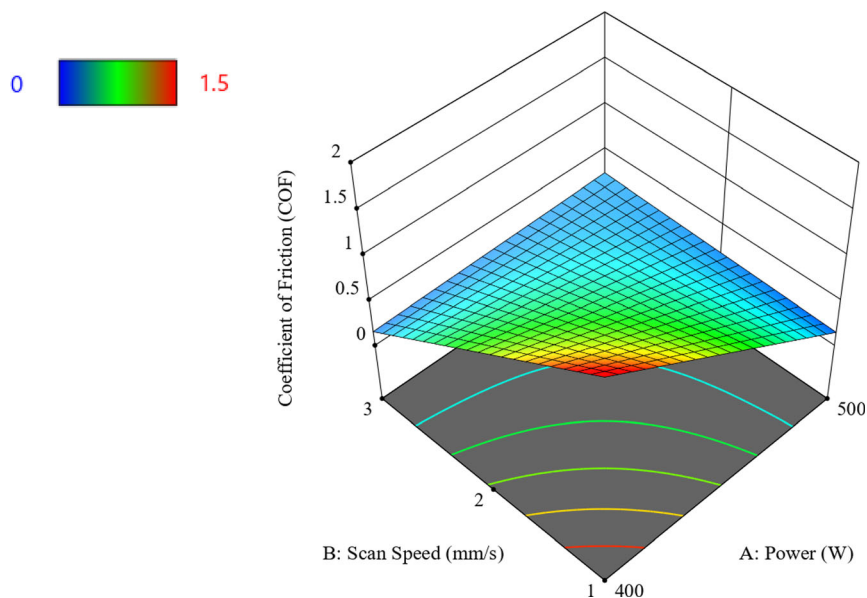


Figure 9. Response graphs showing the effect of the input processing parameters of laser hardening parameters such as laser power (W) and scan speed (mm s^{-1}) on average friction coefficient for all Al 7075 samples.

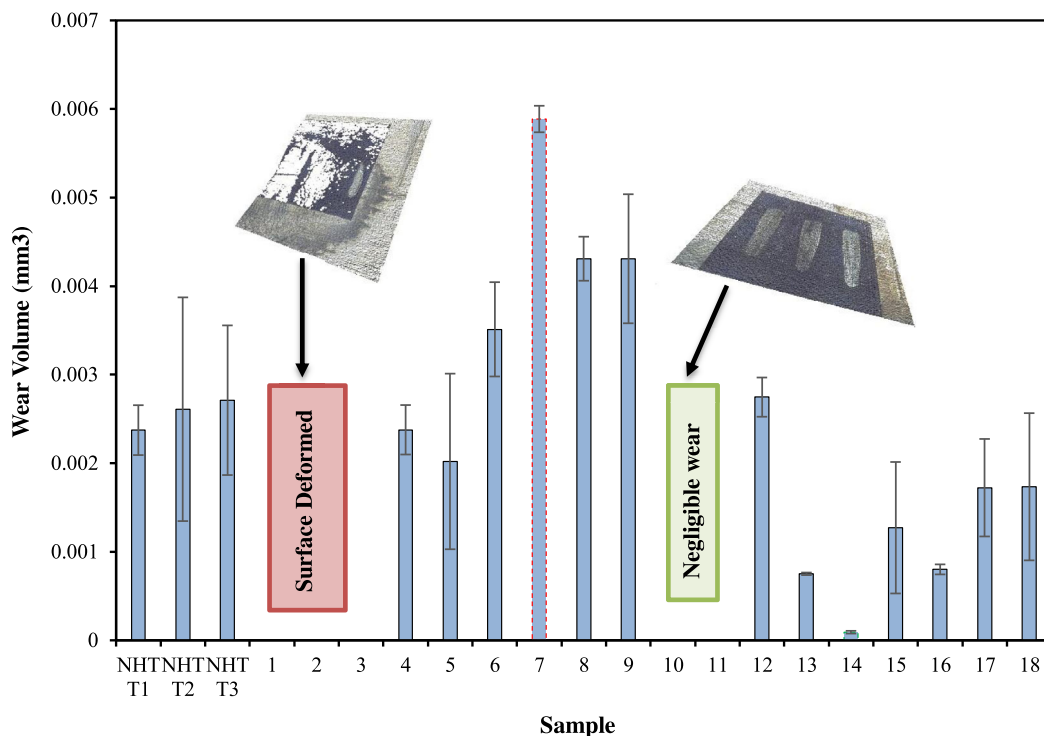


Figure 10. Measured wear volumes of each laser textured and hardened sample. Error bars shown are 95% CIs ($n = 3$). In picture, surface topographies for deformed surface and negligible wear conditions are shown.

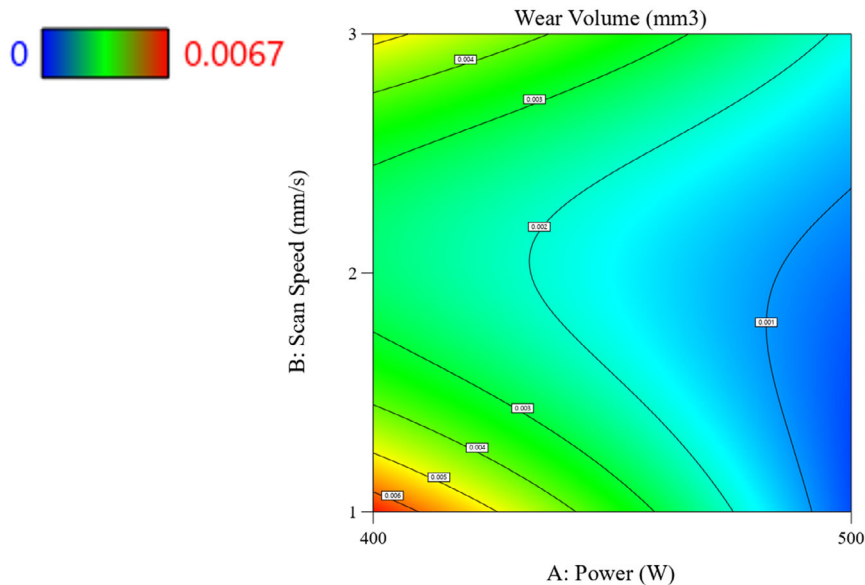


Figure 11. Response contour plots showing the effect of the input processing parameters of laser hardening parameters such as laser power (W) and scan speed (mm s^{-1}) on average friction coefficient for all Al 7075 samples.

correlation coefficients. By using these coefficients, we aimed to understand the strength and direction of correlations among multiple variables such as surface roughnesses S_a , S_q , S_{ku} , S_{sk} , microhardness, COF, and wear volumes. This information was visualized through a heat map displayed in **Figure 12**, which illustrates the

correlations between the input process parameters and the response variables. Further analysis of these correlations, along with scatter plots, can be found in the Supporting Information.

This heat map is an indicator of which laser parameters can be used especially to increase the hardness and reduce the COF and

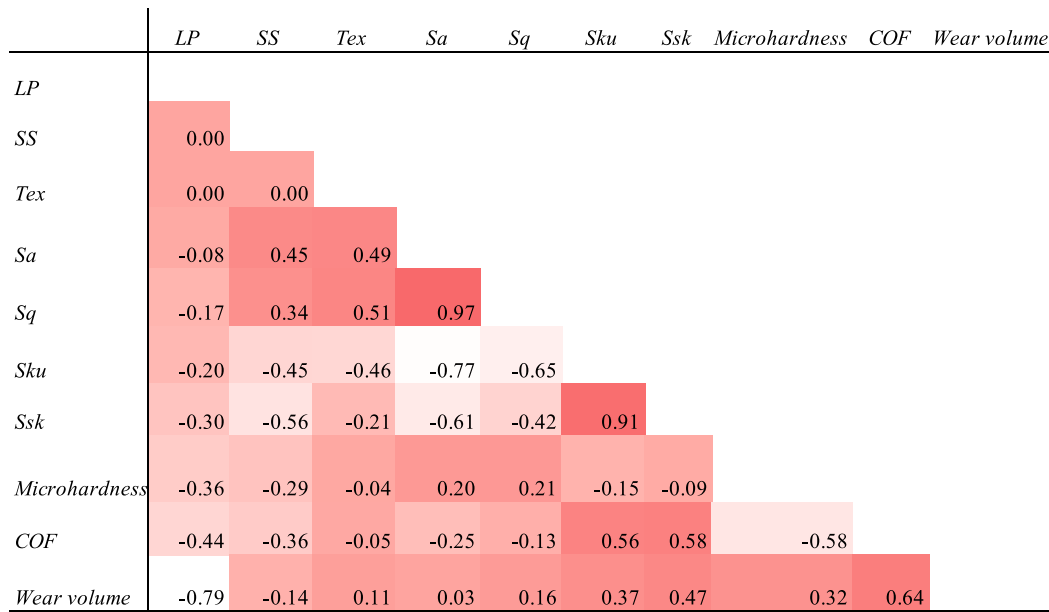


Figure 12. Heat map showing the correlation between input (laser power, scan speed, and texture) and output (S_a , S_q , S_{ku} , S_{sk} , microhardness, COF, and wear volume).

wear volume. With this, the relationship between the laser process parameters and their hardness and wear resistance is established. The scatter plots of correlation coefficient for input and output are provided in the Supporting Information.

4. Conclusion

In conclusion, the multimodal laser texturing–hardening processing strategy offers a simultaneous fabrication of surface textures using an ultrafast laser system and a hardened layer using CW laser on aluminum alloy 7075 surfaces. This approach increases wear performance through the synergistic effects from both the surface texturing and induced hardening. The experimental findings substantiate the effectiveness of this approach. The main conclusions are as follows: 1) The laser texturing and hardening method generated a unique multi-scale surface texture, enhancing mechanical properties and wear resistance. Notably, there was an augmented formation of an aluminum oxide layer on the treated aluminum alloy 7075 surfaces. Furthermore, the treated specimens exhibited lower surface roughness compared to untreated ones. Through meticulous analysis of laser process parameters, a correlation was established, leading to the identification of optimal settings. The optimal process parameters were found to be 500 W, 2 mm s⁻¹, and T1, the star texture pattern. These settings effectively mitigated undesirable defects such as distortion, ensuring the fabrication of high-quality specimens with enhanced performance characteristics. 2) The microhardness evaluation demonstrated a combination of hardening and softening effects on the laser-textured and hardened specimens. Specifically, the microhardness of the hardest sample exhibited a notable increase of 17.8% in comparison with the pristine sample. A regression model was developed using the response surface method which established a

relationship between the hardness and process parameters such as laser power and scan speed. Laser power is the most influential factor affecting microhardness. 3) The predominant wear mechanism observed across all specimens, including both untreated and laser surface textured and hardened specimens, entailed sliding wear, characterized by a synergistic interplay of adhesive and abrasive wear mechanisms, alongside surface smoothing effects. The wear performance was evaluated by analyzing the wear volume and average COF. Notably, the overall average friction coefficient on the laser-textured and heat-treated sample was reduced by 83% compared to the non-heat-treated sample. 4) The wear volumes were characterized in which the most hardened sample had an 80% reduction in wear compared to the non-hardened textured samples. 5) The regression models were developed using the response surface method which established the relationship between the average COF, wear volume, and the laser process parameters, thus allowing tuning of the wear characteristics and enhancing the tribological performance.

In summary, the presented multimodal laser processing strategy examined offers a new approach to surface modification, enhancing both mechanical properties and wear resistance of aluminum alloy 7075 surfaces. This work contributes to the understanding of laser-induced surface modifications and their impact on material performance. Interesting future research directions include exploring the effects of the optimized process parameters of the multimodal laser treatment at the microstructural level. Specifically, examining changes in grain boundaries and phase transformations will provide deeper insights into the mechanisms driving surface hardening and texture formation. Additionally, the corrosion resistance of aluminum alloy 7075 treated with the optimized laser parameters and the effect of phase type and orientation on this electrochemical phenomenon warrants further investigation.

Supporting Information

Supporting Information is available from the Wiley Online Library or from the author.

Acknowledgements

This publication has emanated from research supported by the European Union's Horizon 2020 Research and Innovation Program under grant agreement No. 862100 (NewSkin), supported by Science Foundation Ireland (SFI) under grant no. 16/RC/3872, and is co-funded under the European Regional Development Fund and by I-Form industry partners.

Conflict of Interest

The authors declare no conflict of interest.

Author Contributions

Abhijit Cholkar: Conceptualization (lead); Data curation (lead); Formal analysis (lead); Investigation (lead); Methodology (lead); Project administration (lead); Validation (lead); Writing—original draft (lead). **Suman Chatterjee:** Conceptualization (equal); Data curation (supporting); Formal analysis (supporting); Investigation (supporting); Methodology (supporting); Validation (supporting); Writing—original draft (supporting). **Sujith Kumar:** Data curation (supporting); Formal analysis (supporting); Investigation (supporting); Methodology (supporting); Validation (supporting); Visualization (supporting); Writing—original draft (supporting). **Marko Sedaček:** Data curation (supporting); Formal analysis (supporting); Investigation (supporting); Validation (supporting); Visualization (supporting). **Bojan Podgornik:** Conceptualization (supporting); Formal analysis (supporting); Investigation (supporting); Resources (supporting); Supervision (supporting); Writing—review and editing (supporting). **David Kinahan:** Funding acquisition (lead); Project administration (supporting); Resources (lead); Supervision (equal); Writing—review and editing (supporting). **Dermot Brabazon:** Funding acquisition (lead); Project administration (equal); Resources (lead); Supervision (lead); Writing—original draft (supporting); Writing—review and editing (lead).

Data Availability Statement

The data that support the findings of this study are available in the supplementary material of this article.

Keywords

hardness, laser hardening, parametric modeling, surface modification, ultrafast laser texturing, wear resistance

Received: May 17, 2024

Revised: July 4, 2024

Published online: August 5, 2024

- [1] D. K. Henry, *Coatings* **2020**, *10*, 1.
 [2] A. Cholkar, R. McCann, G. Perumal, S. Chatterjee, M. Swayne, D. Kinahan, D. Brabazon, *Appl. Surf. Sci. Adv.* **2023**, *18*, 100513.
 [3] Y. Li, C. Ning, *Bioact. Mater.* **2019**, *4*, 189.
 [4] A. Cholkar, S. Chatterjee, C. Richards, É. McCarthy, G. Perumal, F. Regan, D. Kinahan, D. Brabazon, *Adv. Mater. Interfaces* **2023**, *2023*, 2300835.

- [5] R. Baumann, Y. Bouraoui, U. Teicher, E. Selbmann, S. Ihlenfeldt, A. F. Lasagni, *Materials* **2023**, *16*, 1205.
 [6] R. Ferreira, Ó. Carvalho, L. Sobral, S. Carvalho, F. Silva, *Friction* **2023**, *11*, 1895.
 [7] M. B. Nandakumar, G. N. Lokesh, H. Natsu, B. R. Mahesh, M. K. Venkatesh, *IOP Conf. Ser. Mater. Sci. Eng.* **2021**, *1013*, 012012.
 [8] L. Hu, H. Fan, W. Cao, T. Hu, *Int. J. Surf. Sci. Eng.* **2021**, *15*, 50.
 [9] A. Arun, P. Lakshmanan, K. Parthiban, G. Kumanan, L. Arunkumar, *Mater. Today Proc.* **2022**, *62*, 615.
 [10] T. Stark, T. Kiedrowski, H. Marschall, A. F. Lasagni, *Lubricants* **2019**, *7*, 1.
 [11] A. Rosenkranz, S. Jaeger, C. Gachot, S. Vogel, F. Mücklich, *Adv. Eng. Mater.* **2015**, *17*, 1208.
 [12] S. Güngör, L. Edwards, *Fatigue Fract. Eng. Mater. Struct.* **1993**, *16*, 391.
 [13] K. Kang, *Wear* **2009**, *266*, 1044.
 [14] Y. Xue, X. Shi, Q. Huang, K. Zhang, C. Wu, *Tribol. Int.* **2021**, *161*, 107099.
 [15] Y. Xue, C. Wu, X. Shi, Q. Huang, A. M. M. Ibrahim, *Friction* **2022**, *10*, 1091.
 [16] S. Athavale, S. Micci-Barreca, K. Arole, V. Kotasthane, J. Blivin, H. Cao, J. L. Lutkenhaus, M. Radovic, M. J. Green, *Langmuir* **2022**, *39*, 918.
 [17] P. D. Babu, K. R. Balasubramanian, G. Buvanashakaran, *Int. J. Surf. Sci. Eng.* **2011**, *5*, 131.
 [18] F. Klocke, M. Schulz, S. Gräfe, *Coatings* **2017**, *7*, 77.
 [19] A. Buling, H. Sändker, J. Stollenwerk, U. Krupp, A. Hamann-Steinmeier, *Appl. Surf. Sci.* **2016**, *378*, 564.
 [20] S. R. Kandavalli, G. B. Rao, P. K. Bannaravuri, M. M. K. Rajam, S. R. Kandavalli, S. R. Ruban, *Mater. Today Proc.* **2021**, *47*, 6919.
 [21] M. A. Tolcha, M. G. Jiru, H. G. Lemu, *Metals* **2021**, *11*, 712.
 [22] V. Kumar, R. Verma, S. Kango, V. S. Sharma, *Mater. Today Commun.* **2021**, *26*, 2352.
 [23] J. Bonse, S. V. Kirner, M. Griepentrog, D. Spaltmann, J. Krüger, *Materials* **2018**, *11*, 801.
 [24] X. Pan, L. Zhou, D. Hu, W. He, P. Liu, Z. Yu, X. Liang, *Appl. Surf. Sci.* **2023**, *636*, 157866.
 [25] M. Sedlaček, B. Podgornik, J. Vižintin, *Wear* **2009**, *266*, 482.
 [26] D. Lisjak, S. Jakovljević, H. Skenderović, *Coatings* **2023**, *13*, 1180.
 [27] T. Liu, C. Guo, L. Zhang, J. Ma, W. Zhang, *Proc. SPIE* **2022**, *12501*, 166.
 [28] A. Abou Khalil, X. Sedao, S. Papa, P. Claudel, A. Klos, T. Itina, N. Attik, A. Guignandon, V. Dumas, in *2021 Conf. Lasers Electro-Opt. Europe Eur. Quant. Electron. Conf. (CLEO/Europe-EQEC)*, IEEE, Munich **2021**.
 [29] A. Čermák, K. Simonović, A. Bondarev, P. Kožmín, Š. Syrovátka, T. Polcar, J. Syrovátka, *Int. J. Adv. Manuf. Technol.* **2022**, *121*, 8479.
 [30] X. Pan, L. Zhou, D. Hu, W. He, P. Liu, Z. Yu, X. Liang, *Appl. Surf. Sci.* **2023**, *636*, 157866.
 [31] A. Cholkar, S. Chatterjee, F. Jose, R. O'Connor, É. McCarthy, N. Weston, D. Kinahan, D. Brabazon, *Int. J. Adv. Manuf. Technol.* **2024**, *130*, 4169.
 [32] Standard (ISO 25178-2:2021) **2021**.
 [33] A. Cholkar, S. Chatterjee, C. Richards, É. McCarthy, G. Perumal, F. Regan, D. Kinahan, D. Brabazon, *Adv. Mater. Interfaces* **2024**, *11*, 2300835.
 [34] O. Khalaj, E. Saebnoori, H. Jirková, O. Chocholatý, L. Kučerová, J. Hajšman, J. Svoboda, *Materials* **2020**, *13*, 5465.
 [35] M. El-Khoury, M. Seifert, S. Bretschneider, M. Zawischa, T. Steege, S. Alamri, A. F. Lasagni, T. Kunze, *Mater. Lett.* **2021**, *303*, 130284.
 [36] M. F. Erinosh, E. T. Akinlabi, O. T. Johnson, *Mater. Res.* **2019**, *22*, e20190297.

- [37] S. Ürgün, T. Canel, *J. Mater. Eng. Perform.* **2023**.
[38] A. Sim, C. Park, N. Kang, Y. Kim, E.-J. Chun, *Surf. Coat. Technol.* **2019**, 377, 124852.
[39] N. Barka, S. S. Karganroudi, R. Fakir, P. Thibeault, V. B. F. Kemda, *Coatings* **2020**, 10, 342.
[40] W. Yi, X. Dang-Sheng, *J. Mater. Process. Technol.* **2007**, 197, 9.
[41] J. Bonse, S. V. Kirner, R. Koter, S. Pentzien, D. Spaltmann, J. Krüger, *Appl. Surf. Sci.* **2017**, 418, 572.
[42] S. Yu, Z. Zhang, Q. Wang, M. Ren, H. Jia, *J. Mater. Process. Technol.* **2023**, 23, 5772.